Author Manuscript

Author Manuscript

Author Manuscript

Author Manuscript

HHS Public Access

Author manuscript

Adv Mater. Author manuscript; available in PMC 2017 February 17.

Published in final edited form as:

Adv Mater. 2016 February 17; 28(7): 1427–1432. doi:10.1002/adma.201504866.

High-performance hydrogen evolution from $MoS_{2(1-x)}P_x$ solid solution

Ruquan Ye, MS,
Department of Chemistry, Rice University, 6100 Main Street, Houston, Texas 77005, USA

Dr. Paz Del Angel Vicente,
Department Physics and Astronomy, University of Texas at San Antonio, One UTSA Circle, San Antonio, Texas 78249, USA

Dr. Yuanyue Liu,
National Renewable Energy Laboratory, Golden, Colorado, 80401, USA

Dr. Josefina Arellano-Jimenez,
Department Physics and Astronomy, University of Texas at San Antonio, One UTSA Circle, San Antonio, Texas 78249, USA

Dr. Zhiwei Peng,
Department of Chemistry, Rice University, 6100 Main Street, Houston, Texas 77005, USA

Tuo Wang, MS,
Department of Chemistry, Rice University, 6100 Main Street, Houston, Texas 77005, USA

Yilun Li, MS,
Department of Chemistry, Rice University, 6100 Main Street, Houston, Texas 77005, USA

Prof. Dr. Boris I. Yakobson,
Department of Chemistry, Rice University, 6100 Main Street, Houston, Texas 77005, USA. Department of Materials Science and NanoEngineering, Rice University, 6100 Main Street, Houston, Texas 77005, USA. Smalley Institute for Nanoscale Science and Technology, Rice University, 6100 Main Street, Houston, Texas 77005, USA

Dr. Su-Huai Wei,
National Renewable Energy Laboratory, Golden, Colorado, 80401, USA

Prof. Dr. Miguel Jose Yacaman, and
Department Physics and Astronomy, University of Texas at San Antonio, One UTSA Circle, San Antonio, Texas 78249, USA

Prof. Dr. James M. Tour
Department of Chemistry, Rice University, 6100 Main Street, Houston, Texas 77005, USA. Department of Materials Science and NanoEngineering, Rice University, 6100 Main Street, Houston, Texas 77005, USA. Smalley Institute for Nanoscale Science and Technology, Rice University, 6100 Main Street, Houston, Texas 77005, USA

Supporting Information Additional data, graphs and equations. Supporting Information is available from the Wiley Online Library or from the author.

Author Manuscript Author Manuscript Author Manuscript Author Manuscript

Abstract

Thermally annealing mixtures of MoS_2 and red phosphorus from 1:0.5 to 1:8 w:w ratio at 750 °C for 1 h under argon/hydrogen leads to the formation of a $MoS_{2(1-x)}P_x$ solid solution (x = 0 to 1). At x = 0.53, the solid solution possesses one of the highest hydrogen evolution reaction (HER) activities of non-precious-metal-based electrocatalysts. The effective and stable electrocatalyst for hydrogen evolution in acidic solution developed here holds promise for substitution of scarce and expensive platinum. The high performance originates from the increased surface area and roughness of the solid solution, as well as the activation of the previously non-active sites as suggested by first–principles calculations. The enhanced HER activity *via* formation of a hetero-anion solid solution may open a new avenue for improving performance of HER and related electrocatalysts.

Graphical Abstract: A MoS

$_{2(1-x)}P_x$ solid solution (x = 0 to 1) is formed by thermally annealing mixtures of MoS_2 and red phosphorus. The effective and stable electrocatalyst for hydrogen evolution in acidic solution holds promise for replacing scarce and expensive platinum that is used in present catalyst systems. The high performance originates from the increased surface area and roughness of the solid solution.

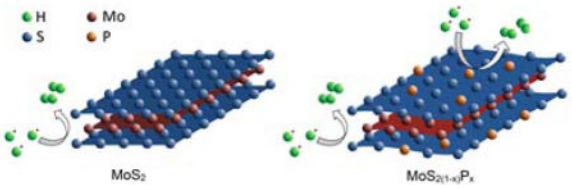

Keywords

hydrogen evolution reaction; electrocatalyst; molybdenum disulfide; molybdenum phosphide; solid solution

Introduction

Research into electrochemical splitting of water to produce hydrogen and oxygen has gained much attention in pursuit of renewable and sustainable energy. Hydrogen as an energy carrier is superior to hydrocarbons in terms of its potential to provide energy security along with environmental and economic benefits.[1,2] However, high-efficiency and cost-effective production of hydrogen remains a technical challenge.[1,3] For example, platinum, as the best hydrogen evolution catalyst, has limited usage due to its scarcity and high price. Molecular biomimetics, which show high hydrogen evolution reaction (HER) activity, are generally non-conductive and air-sensitive, and require the use of sacrificial agents, limiting their sustainable production of hydrogen.[4–6] Therefore, the development of non-precious metal catalysts that drive HER reactions at low overpotential with high reaction rates is critical for the large-scale production of hydrogen through water splitting.

Author Manuscript Author Manuscript Author Manuscript Author Manuscript

Transition metal semiconductor materials, such as dichalcogenides and phosphides, have been used extensively in electrochemical water splitting. Since molybdenum disulfide (MoS_2) is more HER active at the edges of its particles,[7] current research to improving the catalytic performance of MoS_2 focuses primarily on physical morphology engineering, such as stained-exfoliation,[8,9] or formation of porous structure,[10] quantum dots[11] and clusters.[12] Another HER catalyst, molybdenum phosphide (MoP) has shown improved HER activity with lower onset HER overpotential when compared to MoS_2.[13–15] Jaramillo and co-workers further enhanced the HER activity and stability of MoP by introducing sulfur to the surface of MoP.[14] However, the mechanism of enhancing the HER catalytic activity was not clarified.

Here, we report a one-step approach to improve the HER activity of MoS_2 and MoP *via* formation of a $MoS_{2(1-x)}P_x$ (x = 0 to 1) solid solution. By annealing bulk particulate MoS_2 (diameter ~ 6 μm) with different amounts of red phosphorus at 750 °C in argon/hydrogen flow, MoS_2 gradually transforms into MoP (See Supporting Methods for details). At x = 0.53, the solid solution MoSP reaches its maximum performance, exhibiting one of the highest HER activities based on non-precious-metal electrocatalysts, yet maintaining excellent stability during durability testing. Increasing the surface area of the solid solution by either mixing with carbon black or using MoS_2 nanoparticles (135 nm) as precursors, leads to further improvement of HER activity. The high HER performance and cost–effective preparation route of the solid solution makes it a potential substituent for Pt in HER. In addition, the technology reported here by formation of a solid solution with hetero-anions may open new avenues to improve the electrocatalytic activity of other transition metal semiconductors.

Result and discussion

Scanning electron microscopy (SEM) images of MoS_2, $MoS_{0.94}P_{0.53}$ and MoP (Figure 1a–c) shows that the MoS_2 particle size is ~ 6 μm, whereas after reaction with phosphorous, the materials become larger. Brunauer–Emmett–Teller (BET) analyses (Figure S1) reveals that the BET surface area of $MoS_{2(1-x)}P_x$ increases gradually from 1.3 $m^2\ g^{-1}$ to 9.4 $m^2\ g^{-1}$ as x increases from 0 to 1, which is consistent with the morphology observation under SEM.

The chemical constituents of $MoS_{2(1-x)}P_x$ were further investigated by X-ray photoelectron spectroscopy (XPS) and X-ray diffraction (XRD) (Figure 1d–f). As depicted in XPS (Figure 1d and Figure S2a), during the reaction with phosphorous, the Mo^{4+} 3d5/2 and Mo^{4+} 3d3/2 peaks at ~ 229.2 eV and ~ 232.4 eV become weaker, yet the Mo^{3+} 3d5/2 and Mo^{3+} 3d3/2 peaks at ~ 228.2 eV and ~ 231.4 eV become more pronounced. The peak intensity for S 2s at ~ 226.2 eV was reduced, which confirms the successful transformation of MoS_2 into MoP. High resolution P 2p and S 2p XPS spectra (Figure 1f) of $MoS_{0.94}P_{0.53}$ resembles that of MoP and MoS_2, indicating a similar oxidation state and elemental environment of P and S in $MoS_{0.94}P_{0.53}$ to that of MoP and MoS_2, respectively. Besides a doublet at ~ 130 eV for P^{3-}, a broad peak at ~ 134 eV was observed, which corresponds to PO_4^{3-}, a peak typical for MoP that has been exposed to air.[13–15] Similar transitions were detected in the XRD patterns. As shown in Figure 1e and Figure S2b, as MoS_2 was converted into MoP, the peak intensities corresponding to MoS_2 declined, whereas those of MoP were amplified. The crystal domain

Author Manuscript Author Manuscript Author Manuscript Author Manuscript

sizes calculated from the crystalline facets of MoS_2 (002) and MoP (101) using the Scherrer equation[16] are summarized in Figure 1g. It can seen that the size of MoS_2 (002) plane changes little, whereas the size of MoP (101) plane increases from ~ 20 nm to 47 nm as x increases.

The HER acitivities of $MoS_{2(1-x)}P_x$ are evaluated in 0.5 M H_2SO_4 using a three-electrode electrochemical cell. Remarkably, bulk MoS_2 shows little HER activity, whereas its performance is greatly improved with partial transformatioin into MoP. The HER activity reaches its maximum at x = 0.53, where an overpotential of ~ 150 mV is needed to deliver a current density of 10 mV cm^{-2}. However, further reaction of $MoS_{0.94}P_{0.53}$ with phosphorous results in a decrease in HER activity, an additional 40 mV and 90 mV are required for $MoS_{0.60}P_{0.70}$ and MoP to reach 10 mV cm^{-2}, respectively.

The HER performance of $MoS_{2(1-x)}P_x$ can be further elevated by increasing the surface active sites of the electrode in two ways. The first one is to introduce a porous conductive substrate onto the electrode. As shown in Figure S3, direct mixing of $MoS_{0.94}P_{0.53}$ with 20% carbon black ($MoS_{0.86}P_{0.57}$/CB) leads to a overpotential deduction of 30 mV to reach 10 mA cm^{-2}. As MoS_2 is only HER active at the edges, the second approach is to use 135 nm MoS_2 nanoparticles as precusors instead of the ~ 6 μm particles. As expected, a three-fold increase of current density at 200 mV overpotential is achieved when using 135 nm MoS_2 nanoparticles as precursors (Figure S3). Similar further enhancement can be obtained when introducing carbon black as a substrate. As summarized in Table S1, the overpotentials for $MoS_{1.4}P_{0.29*}$/CB to deliver current densities of 10 mA cm^{-2} and 20 mA cm^{-2}, are much lower than those electrodes prepared at similar sample loadings, and among the best performing materials based on non-precious metal based catalysts. However, direct physical mixing MoS_2 and MoP in a mass ratio of 1:1 or 1:4 does not lead to synergistically enhanced HER performance. As shown in Figure S4, although the elemental composition of these mixtures resembles that of $MoS_{0.94}P_{0.53}$ and $MoS_{0.60}P_{0.70}$, respectively, both ratios of mixtures display lower current densities than that of MoP.

The stability of the catalyst was examined by measuring 20000 continuous linear sweeps between −0.3 and 0.25 V (*vs* RHE) in 0.5 M H_2SO_4 at a scan rate of 100 mV s^{-1}. As shown in Figure S5a, the current density between −0.17 and 0.2 V, which corresponds to the reduction of PO_4^{3-} to P^{3-}, becomes lower during the cyclability test. As shown in the inset of Figure S5a, the overpotential needed to maintain the same current density decreases during the first 2000 cycles, whereas it increases slightly after 20000 cycles. As to MoP, the HER activity is enhanced after 20000 cycles (Figure S5b). This indicates that the electrocatalysts prepared by phosphorous displacement in this work are stable in the acidic electrolyte.

The intrinsic HER activities of $MoS_{2(1-x)}P_x$ were assessed by studying Tafel slopes and the hydrogen turnover frequency (TOF), which is the number of hydrogen molecules evolved per second per active site. Tafel analysis (Figure 2b and Figure 2c) reveals that reaction with phosphorous significantly reduces the Tafel slope from 131 mV $decade^{-1}$ (MoS_2) to 57 mV $decade^{-1}$ ($MoS_{0.60}P_{0.70}$), indicating the HER shifted to a Volmer-Heyrovsky pathway, a more HER-favorable mechanism.[12,17] To elucidate the TOF values of $MoS_{2(1-x)}P_x$, we first

Author Manuscript Author Manuscript Author Manuscript Author Manuscript

evaluate the number of active sites from the electrochemical active surface area (ECSA), a method generally used to estimate the active sites for transition metal semiconductors[14,18,19] (Figure S6 and Supporting Equations). As shown in Figure S6 and Table S2, the electrochemical surface area (ECSA) of $MoS_{2(1-x)}P_x$ increases greatly from $0.128\,cm^2_{ECSA}$ for MoS_2, to $140\,cm^2_{ECSA}$ for MoP, an increase that is consistent with the increase of BET surface area observed previously (Figure S2). The hydrogen TOF values calculated from the ECSA and polarization curves are plotted in Figure 2d together with those of Ni_2P[19], MoP[14], MoP|S[14] and $[Mo_3S_{13}]^{2-}$[12] for comparison. Although the ECSA increases with the degree of phosphorous reaction, the TOF value reaches a maximum for $MoS_{0.94}P_{0.53}$. At x = 0.53, $MoS_{2(1-x)}P_x$ displays a TOF of 0.83 $H_2\ s^{-1}$ and 1.4 $H_2\ s^{-1}$ at 100 mV and 200 mV overpotential, respectively, which are among the highest values for non-precious-metal catalysts.

To probe the possible reasons for the high HER performance of $MoS_{2(1-x)}P_x$, an aberration-corrected scanning transmission electron microscopy (STEM) was used to investigate the atomic structure of the solid solution. Figures 3a–c are the high angle annular dark field (HAADF) STEM images of MoS_2, which display a clear layered structure at the edge (Figure 3a) and hexagonal structure on the basal planes (Figure 3b and Figure 3c), characteristic of the materials. However, reaction with phosphorous leads to a more disordered structure and irregular morphology. As shown in Figure 3d, the bright field (BF) STEM image of $MoS_{0.94}P_{0.53}$ becomes much more irregular as compared to that of Figure 3b, indicating a phase transition after reaction with phosphorous. Different structures showing diverse degrees of disorder can be observed through higher resolution STEM images. For example, the surface brightness (Figure 3e) becomes much more irregular, indicating a different thickness on the materials' surface. In some regions, a strained basal plane can be found, as indicated in Figure 3f where the atoms depart from the MoS_2 hexagonal lattice. The partial deformation of the pristine MoS_2 crystalline structure after phosphorous incorporation (Figures 3,f) indicates the substitution of S by P in the MoS_2 lattice. However, whether the displacement is randomly distributed or partially concentrated cannot be concluded due to the similarity of the Mo-S and Mo-P bond lengths. Elemental mapping by energy-dispersive-X-ray-spectroscopy (EDS)-STEM of $MoS_{0.94}P_{0.53}$ (Figure 3g–j, Figure S7) shows that Mo, P and S are mostly homogeneously distributed among the sample, except the region with low P (circled in Figure h–j). The linear scan atomic composition corresponding to the line profile in Figure 3g is summarized in Figure 3k. It can be seen that the atomic composition of S to P is mostly ~ 2:1, consistent with the XPS result. The partial inhomogeneity is attributed to poor mixing of MoS_2 and red phosphorus. However, as MoS_2 is transformed into MoP by increasing the phosphorous ratio in the precursor mixture, the original MoS_2 layered structure is lost (Figure 3l); instead, a non-planar well-crystallized material is observed. The atomic composition derived from EDS analysis further confirms that the composition is ~ 1:1 Mo:P (Figure S8 and Table S3).

The BET surface area analysis and STEM images reveal that the transformation of MoS_2 to MoP increases surface roughness and surface area with x. The HER activity of the solid solution reaches its maximum at x = 0.53, and physical mixing of MoS_2 and MoP does not increase the HER activity (Figure S4).

Author Manuscript Author Manuscript Author Manuscript Author Manuscript

To understand the origin of the improvement of HER activity by P-alloying, we performed density functional theory (DFT) calculations using projector augmented wave (PAW) pseudopotentials[20,21] and Perdew–Burke–Ernzerhof (PBE) exchange-correlation functional[22] as implemented in the Vienna *ab initio* Simulation Package (VASP).[23,24] A supercell composed of 6 × 6 MoS_2 primitive cells was used to model the P-alloying and H adsorption.

The free energy of H adsorption, which represents the energy benefit/cost to adsorb one H on the catalyst and therefore reflects the kinetics of HER, is defined in eq 1:

$$G_{\mathrm{H}}=G(\mathrm{cata+H})-G(\mathrm{cata})-1/2G(\mathrm{H_2}) \quad (1)$$

where G(cata), G(cata+H) and $G(H_2)$ are the free energy of the catalyst, H is the adsorbed hydrogen atom, and H_2 is a hydrogen molecule, respectively. According to Sabatiers' principle, the closer to zero the G_{diff} is, the higher HER activity it will have.[25] We find that G_H = 2.2 eV for the pristine MoS_2 surface (Figure 4a, dashed line), suggesting that the pristine surface is not active, in agreement with the common belief that MoS_2 is only edge active.[26] However, as shown in Figure 4a, P-alloying causes a significant drop of G_H for neighboring S atoms to < 0.8 eV, indicating that MoS_2 becomes surface active.

The enhanced H adsorption on the MoS_2 surface induced by P-alloying can be explained by using the 'states-filling' model[27] where the binding energy between the adsorbate and the substrate correlates with the work required to fill previously unoccupied electronic states within the substrate. The easier the electrons can be filled, the stronger the binding. For the pristine MoS_2 surface, the first available state for H electron occupation is the conduction band minimum (CBM), which is ~ 1.7 eV above the valence band maximum (VBM). In contrast, P-alloying creates a shallow unoccupied state (Figure 4b left, the nearly flat band shown in red) that is only ~ 0.17 eV above the VBM. This level can accept the electron of the H after its adsorption (Figure 4b right). Therefore, the work required to accommodate the H electron is much lower in the P-alloyed case than that of a pristine surface, leading to a stronger H binding. This finding is similar to a recent result by others on the study of cobalt phosphosulphide.[28]

Conclusion

We have demonstrated a simple method to improve the HER activity of transition metal semiconductors *via* the formation of a solid solution. The HER activity of the solid solution can be further improved by increasing the surface area, such as employing MoS_2 nanoparticles as precursor, or adding carbon black as a substrate. We note that there is still room for additional enhancement of the solid solution, such as manipulating with smaller sizes of MoS_2 precursor and using high-surface-area heteroatom-alloyed carbon support.[17,29–31] The formation of a solid solution leads to an increase in surface roughness and ECSA of the materials. In addition, theoretical calculation suggests that substitution of sulfur by phosphorus improves the HER catalytic activity of the MoS_2 basal plane. The

Author Manuscript Author Manuscript Author Manuscript Author Manuscript

method developed here may also have influence on the development of other catalysts, especially semiconductors that are based on transition metals such as Co, Ni and W.

Supplementary Material

Refer to Web version on PubMed Central for supplementary material.

Acknowledgments

The Air Force Office of Scientific Research (FA9550-14-1-0111) partially funded this work. Work at NREL was supported by U.S. DOE under Contract No. DE-AC36-08GO28308. The work at UTSA was supported by the National Center for Research Resources (5 G12RR013646-12), NSF-PREM (DMR 0934218) and the National Institute on Minority Health and Health Disparities (G12MD007591) from the National Institutes of Health.

References

1. Thomas, G. Overview of Storage Development - DOE Hydrogen Program. Sandia National Laboratories; 2000.
2. Mazloomi K, Gomes C. Renewable & Sustainable Energy Reviews. 2012; 16:3024.
3. Amoo LM, Fagbenle RL. Int J Hydrogen Energy. 2014; 39:12409.
4. Berggren G, Adamska A, Lambertz C, Simmons TR, Esselborn J, Atta M, Gambarelli S, Mouesca JM, Reijerse E, Lubitz W, Happe T, Artero V, Fontecave M. Nature. 2013; 499:66. [PubMed: 23803769]
5. Rauchfuss TB. Science. 2007; 317:43. [PubMed: 17615325]
6. Le Goff A, Artero V, Jousselme B, Tran PD, Guillet N, Metaye R, Fihri A, Palacin S, Fontecave M. Science. 2009; 326:1384–1387. [PubMed: 19965754]
7. Jaramillo TF, Jorgensen KP, Bonde J, Nielsen JH, Horch S, Chorkendorff I. Science. 2007; 317:100. [PubMed: 17615351]
8. Lukowski MA, Daniel AS, Meng F, Forticaux A, Li LS, Jin S. J Am Chem Soc. 2013; 135:10274. [PubMed: 23790049]
9. Ji S, Yang Z, Zhang C, Liu Z, Tjiu W, Phang IY, Zhang Z, Pan JS, Liu T. Electrochim Acta. 2013; 109:269.
10. Kibsgaard J, Chen Z, Reinecke BN, Jaramillo TF. Nat Mater. 2012; 11:963. [PubMed: 23042413]
11. Gopalakrishnan D, Damien D, Shaijumon MM. ACS Nano. 2014; 8:5297. [PubMed: 24773177]
12. Kibsgaard J, Jaramillo TF, Besenbacher F. Nat Chem. 2014; 6:248. [PubMed: 24557141]
13. Xiao P, Sk MA, Thia L, Ge XM, Lim RJ, Wang JY, Lim KH, Wang X. Energy Environ Sci. 2014; 7:2624.
14. Kibsgaard J, Jaramillo TF. Angew Chem Int Ed. 2014; 53:14433.
15. Xing Z, Liu Q, Asiri AM, Sun X. Adv Mater. 2014; 26:5702. [PubMed: 24956199]
16. Langford JI, Wilson AJC. J Appl Crystallogr. 1978; 11:102.
17. Li Y, Wang H, Xie L, Liang Y, Hong G, Dai H. J Am Chem Soc. 2011; 133:7296. [PubMed: 21510646]
18. Popczun EJ, Read CG, Roske CW, Lewis NS, Schaak RE. Angew Chem Int Ed. 2014; 53:5427.
19. Popczun EJ, McKone JR, Read CG, Biacchi AJ, Wiltrout AM, Lewis NS, Schaak RE. J Am Chem Soc. 2013; 135:9267. [PubMed: 23763295]
20. Blöchl PE. Phys Rev B. 1994; 50:17953.
21. Kresse G, Joubert D. Phys Rev B. 1999; 59:1758.
22. Perdew JP, Burke K, Ernzerhof M. Phys Rev Lett. 1996; 77:3865. [PubMed: 10062328]
23. Kresse G, Hafner J. Phys Rev B. 1993; 47:558.
24. Kresse G, Furthmüller J. Phys Rev B. 1996; 54:11169.
25. Nørskov JK, Bligaard T, Logadottir A, Kitchin JR, Chen JG, Pandelov S, Stimming U. J Electrochem Soc. 2005; 152:J23.

Author Manuscript Author Manuscript Author Manuscript Author Manuscript

26. Jaramillo TF, Jørgensen KP, Bonde J, Nielsen JH, Horch S, Chorkendorff I. Science. 2007; 317:100. [PubMed: 17615351]
27. Liu Y, Wang YM, Yakobson BI, Wood BC. Phys Rev Lett. 2014; 113:028304. [PubMed: 25062244]
28. Cabán-Acevedo, M., Stone, ML., Schmidt, JR., Thomas, JG., Ding, Q., Chang, H., Tsai, M., He, J., Jin, S. Nat Mater. ASAP; 2015. http://dx.doi.org/10.1038/nmat4410
29. Chen S, Duan J, Tang Y, Jin B, Qiao S. Nano Energy. 2015; 11:11.
30. Wang J, Wang G, Miao S, Li JY, Bao X. Faraday Discuss. 2014; 176:135. [PubMed: 25612219]
31. Lauritsen JV, Kibsgaard J, Helveg S, Topsoe H, Clausen BS, Laegsgaard E, Besenbacher F. Nat Nanotechnol. 2007; 2:53. [PubMed: 18654208]

Author Manuscript Author Manuscript Author Manuscript Author Manuscript

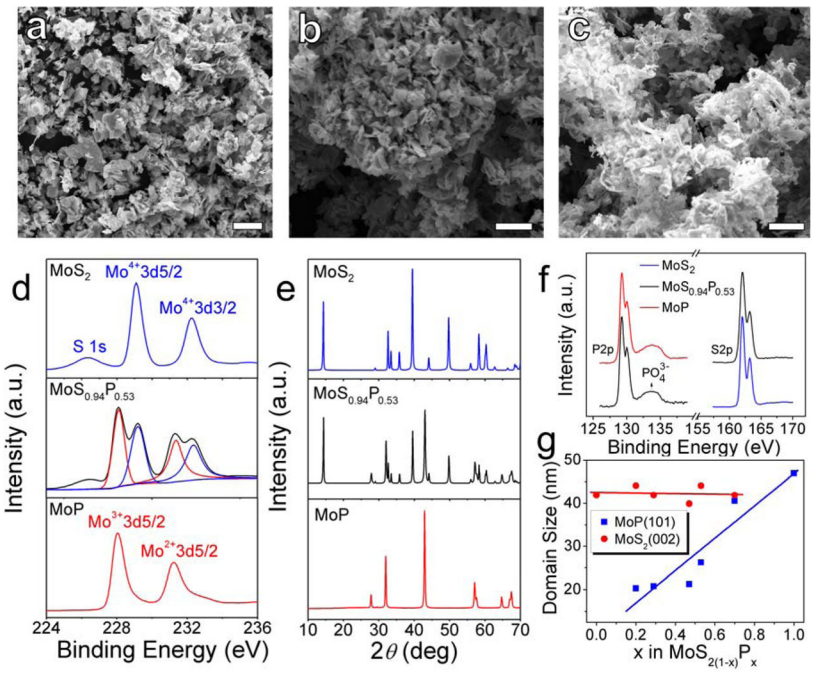

Figure 1. Structure characterization of $MoS_{2(1-x)}P_x$

SEM images of (a) MoS_2, (b) $MoS_{0.94}P_{0.53}$ and (c) MoP. The scale bars are 10 μm. (d) High resolution XPS spectra of Mo3d. (e) XRD spectra of MoS_2, $MoS_{0.94}P_{0.53}$ and MoP. (f) High resolution XPS P2p and S2p spectra of MoS_2 (blue line), $MoS_{0.94}P_{0.53}$ (black line) and MoP (red line). (g) Domain sizes of MoS_2 (002) plane and MoP (101) plane in $MoS_{2(1-x)}P_x$.

Author Manuscript Author Manuscript Author Manuscript Author Manuscript

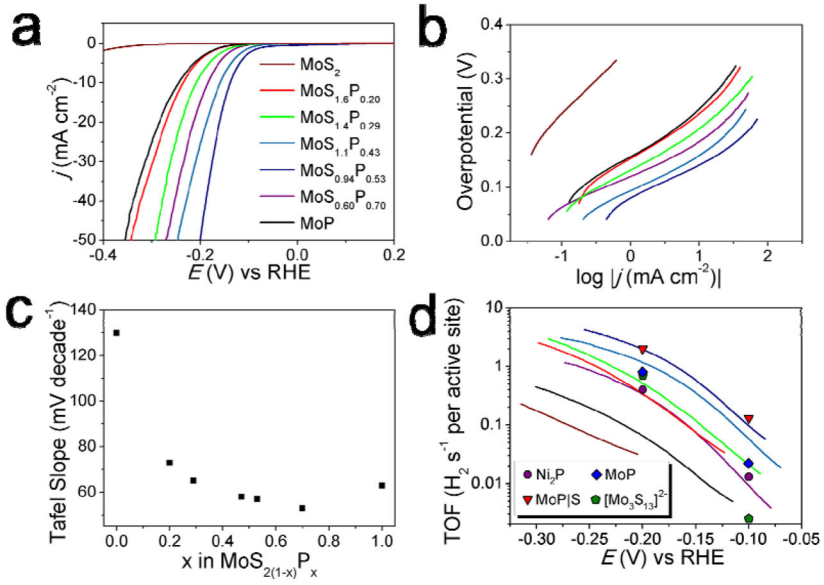

Figure 2. HER catalytic activity of $MoS_{2(1-x)}P_x$

(a) Linear sweep polarization curves of $MoS_{2(1-x)}P_x$ in 0.5 M H_2SO_4. The sample loading are ~ 0.285 mg cm^{-2} and the scan rates are 5 mV s^{-1}. (b) Tafel plots of $MoS_{2(1-x)}P_x$. (c) Summary of the Tafel slopes with change of x in $MoS_{2(1-x)}P_x$. (d) TOF values of $MoS_{2(1-x)}P_x$ using 40 μF cm^{-2} as the specific capacitance stardard. The TOF values for Ni_2P,[19] MoP,[14] MoP|S[14] and $[Mo_3S_{13}]^{2-}$[12] from the literature are displayed for comparison. The legend colors in Figure 2b and Figure 2d are the same as that in Figure 2a.

Author Manuscript Author Manuscript Author Manuscript Author Manuscript

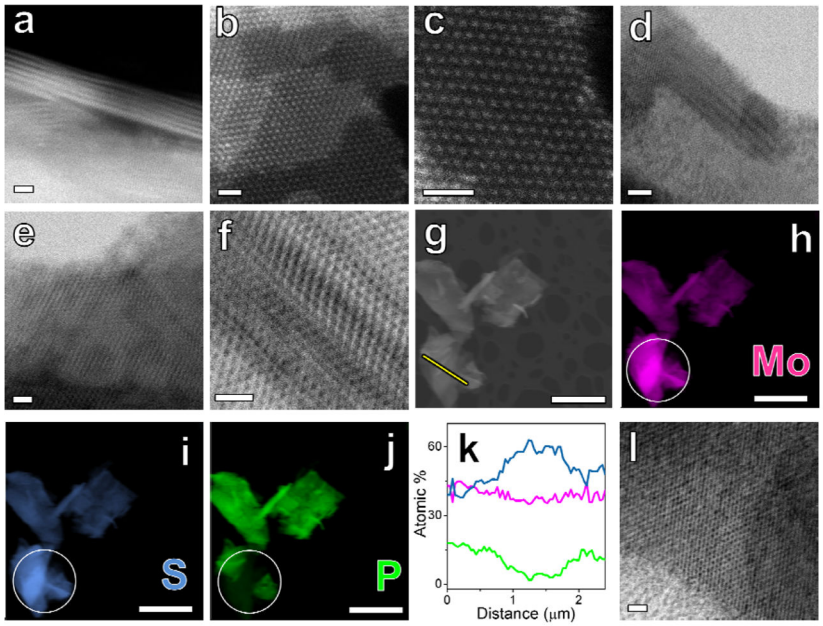

Figure 3. STEM images of $MoS_{2(1-x)}P_x$

HAADF-STEM images of MoS_2 showing (a) the layers and (b) basal plane structure. (c) Higher resolution characteristic MoS_2 basal plane structure. (d–f) BF-STEM images of $MoS_{0.94}P_{0.53}$ showing roughness and disorder on the surface. (g–j) Elemental mapping from EDS-STEM of $MoS_{0.94}P_{0.53}$ sample; (g) is the raw STEM image and (h), (i), (j) are the elemental distribution of Mo, S and P, respectively. The circled areas in h-j represent a region with lower P composition. (k) Linear scan atomic composition of $MoS_{0.94}P_{0.53}$ along the yellow line in (g). Mo (red); S (blue); P (green). (l) BF-STEM image of MoP showing a non-planar well-crystallized structure. The scale bars are 2 nm in a and d; 1 nm in b, c, e, f and l; 2 μm in g–j.

Author Manuscript Author Manuscript Author Manuscript Author Manuscript

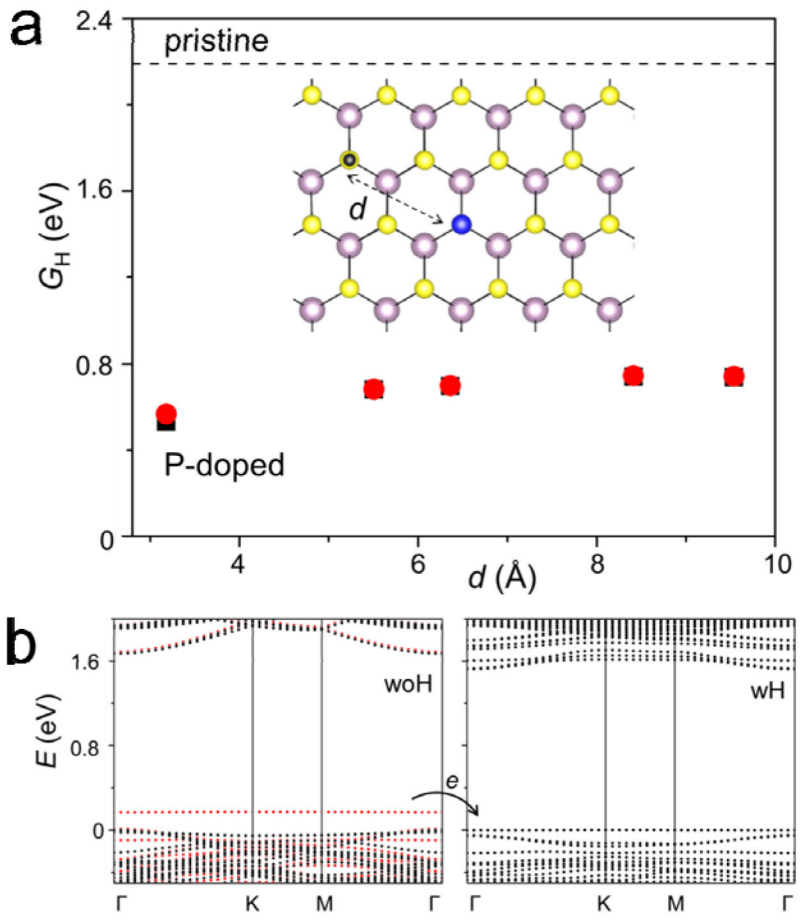

Figure 4. Enhanced HER activity simulated from DFT calculations

(a) Free energy of H adsorption on pristine MoS_2 surface (dashed line), and on P-alloyed surface (dots) as a function of the in-plane distance between H and P. Black dots are for the H adsorbed on the same side as P, and red dots are for the H absorbed on the other side. The inset shows the structure of a P (blue) atom substituting the S atom, with H (black) adsorbed on neighboring S (Mo atoms are purple). (b) Band structure of a P-alloyed MoS_2 without (left) and with (right) H adsorption. The spins in P- alloyed MoS_2 are polarized, and are shown by black and red dots, respectively. After H adsorption, the H transfers its electron to P, and the system becomes spin degenerate.